2002MNRAS.336..483I

Mon. Not. R. Astron. Soc. **336,** 483–500 (2002)

Long-term integrations and stability of planetary orbits in our Solar system

Takashi Ito★ and Kiyotaka Tanikawa

Data Analysis Center and Theoretical Astrophysics Division, National Astronomical Observatory, Mitaka, Tokyo 181-8588, Japan

Accepted 2002 June 10. Received 2002 May 23; in original form 2001 November 19

ABSTRACT

We present the results of very long-term numerical integrations of planetary orbital motions over 10^9-yr time-spans including all nine planets. A quick inspection of our numerical data shows that the planetary motion, at least in our simple dynamical model, seems to be quite stable even over this very long time-span. A closer look at the lowest-frequency oscillations using a low-pass filter shows us the potentially diffusive character of terrestrial planetary motion, especially that of Mercury. The behaviour of the eccentricity of Mercury in our integrations is qualitatively similar to the results from Jacques Laskar's secular perturbation theory (e.g. $e_{\max} \sim 0.35$ over $\sim \pm 4$ Gyr). However, there are no apparent secular increases of eccentricity or inclination in any orbital elements of the planets, which may be revealed by still longer-term numerical integrations. We have also performed a couple of trial integrations including motions of the outer five planets over the duration of $\pm 5 \times 10^{10}$ yr. The result indicates that the three major resonances in the Neptune–Pluto system have been maintained over the 10^{11}-yr time-span.

Key words: celestial mechanics – Solar system: general.

1 INTRODUCTION

1.1 Definition of the problem

The question of the stability of our Solar system has been debated over several hundred years, since the era of Newton. The problem has attracted many famous mathematicians over the years and has played a central role in the development of non-linear dynamics and chaos theory. However, we do not yet have a definite answer to the question of whether our Solar system is stable or not. This is partly a result of the fact that the definition of the term 'stability' is vague when it is used in relation to the problem of planetary motion in the Solar system. Actually it is not easy to give a clear, rigorous and physically meaningful definition of the stability of our Solar system.

Among many definitions of stability, here we adopt the Hill definition (Gladman 1993): actually this is not a definition of stability, but of instability. We define a system as becoming unstable when a close encounter occurs somewhere in the system, starting from a certain initial configuration (Chambers, Wetherill & Boss 1996; Ito & Tanikawa 1999). A system is defined as experiencing a close encounter when two bodies approach one another within an area of the larger Hill radius. Otherwise the system is defined as being stable. Henceforward we state that our planetary system is dynamically stable if no close encounter happens during the age of our Solar system, about ± 5 Gyr. Incidentally, this definition may be replaced by one in which an occurrence of any orbital crossing between either of a pair of planets takes place. This is because we know from experience that an orbital crossing is very likely to lead to a close encounter in planetary and protoplanetary systems (Yoshinaga, Kokubo & Makino 1999). Of course this statement cannot be simply applied to systems with stable orbital resonances such as the Neptune–Pluto system.

1.2 Previous studies and aims of this research

In addition to the vagueness of the concept of stability, the planets in our Solar system show a character typical of dynamical chaos (Sussman & Wisdom 1988, 1992). The cause of this chaotic behaviour is now partly understood as being a result of resonance overlapping (Murray & Holman 1999; Lecar, Franklin & Holman 2001). However, it would require integrating over an ensemble of planetary systems including all nine planets for a period covering several 10 Gyr to thoroughly understand the long-term evolution of planetary orbits, since chaotic dynamical systems are characterized by their strong dependence on initial conditions.

From that point of view, many of the previous long-term numerical integrations included only the outer five planets (Sussman & Wisdom 1988; Kinoshita & Nakai 1996). This is because the orbital periods of the outer planets are so much longer than those of the inner four planets that it is much easier to follow the system for a given integration period. At present, the longest numerical integrations

★E-mail: tito@cc.nao.ac.jp

© 2002 RAS

© Royal Astronomical Society • Provided by the NASA Astrophysics Data System

2002MNRAS.336..483I

published in journals are those of Duncan & Lissauer (1998). Although their main target was the effect of post-main-sequence solar mass loss on the stability of planetary orbits, they performed many integrations covering up to $\sim 10^{11}$ yr of the orbital motions of the four jovian planets. The initial orbital elements and masses of planets are the same as those of our Solar system in Duncan & Lissauer's paper, but they decrease the mass of the Sun gradually in their numerical experiments. This is because they consider the effect of post-main-sequence solar mass loss in the paper. Consequently, they found that the crossing time-scale of planetary orbits, which can be a typical indicator of the instability time-scale, is quite sensitive to the rate of mass decrease of the Sun. When the mass of the Sun is close to its present value, the jovian planets remain stable over 10^{10} yr, or perhaps longer. Duncan & Lissauer also performed four similar experiments on the orbital motion of seven planets (Venus to Neptune), which cover a span of $\sim 10^9$ yr. Their experiments on the seven planets are not yet comprehensive, but it seems that the terrestrial planets also remain stable during the integration period, maintaining almost regular oscillations.

On the other hand, in his accurate semi-analytical secular perturbation theory (Laskar 1988), Laskar finds that large and irregular variations can appear in the eccentricities and inclinations of the terrestrial planets, especially of Mercury and Mars on a time-scale of several 10^9 yr (Laskar 1996). The results of Laskar's secular perturbation theory should be confirmed and investigated by fully numerical integrations.

In this paper we present preliminary results of six long-term numerical integrations on all nine planetary orbits, covering a span of several 10^9 yr, and of two other integrations covering a span of $\pm 5 \times 10^{10}$ yr. The total elapsed time for all integrations is more than 5 yr, using several dedicated PCs and workstations. One of the fundamental conclusions of our long-term integrations is that Solar system planetary motion seems to be stable in terms of the Hill stability mentioned above, at least over a time-span of ± 4 Gyr. Actually, in our numerical integrations the system was far more stable than what is defined by the Hill stability criterion: not only did no close encounter happen during the integration period, but also all the planetary orbital elements have been confined in a narrow region both in time and frequency domain, though planetary motions are stochastic. Since the purpose of this paper is to exhibit and overview the results of our long-term numerical integrations, we show typical example figures as evidence of the very long-term stability of Solar system planetary motion. For readers who have more specific and deeper interests in our numerical results, we have prepared a web-page (access http://www.cc.nao.ac.jp/~tito/articles/MNRAS2002/), where we show raw orbital elements, their low-pass filtered results, variation of Delaunay elements and angular momentum deficit, and results of our simple time–frequency analysis on all of our integrations.

In Section 2 we briefly explain our dynamical model, numerical method and initial conditions used in our integrations. Section 3 is devoted to a description of the quick results of the numerical integrations. Very long-term stability of Solar system planetary motion is apparent both in planetary positions and orbital elements. A rough estimation of numerical errors is also given. Section 4 goes on to a discussion of the longest-term variation of planetary orbits using a low-pass filter and includes a discussion of angular momentum deficit. In Section 5, we present a set of numerical integrations for the outer five planets that spans $\pm 5 \times 10^{10}$ yr. In Section 6 we also discuss the long-term stability of the planetary motion and its possible cause.

2 DESCRIPTION OF THE NUMERICAL INTEGRATIONS

2.1 Equations of motion

We consider the planetary system as a non-linear Hamiltonian system, governed only by classical Newtonian gravitational force between the planets and the Sun. The equation of motion in the inertial space is

$$\frac{\mathrm{d}^2 \boldsymbol{x}_i}{\mathrm{d}t^2} = -\sum_{\substack{j=0 \\ j \neq i}}^{N} \frac{G m_j}{|\boldsymbol{x}_i - \boldsymbol{x}_j|^3} (\boldsymbol{x}_i - \boldsymbol{x}_j) + \boldsymbol{a}_i, \tag{1}$$

where i denotes the index for each celestial body (Sun, Mercury, Venus, ... , Pluto), $\boldsymbol{x}_i$ is the position and m_i is the mass of the ith particle in the inertial space. G is the gravitational constant, $N(=9)$ is the number of particles and $\boldsymbol{a}_i$ represents any small extra acceleration arising from sources other than Newtonian gravitational interactions between the planets and the Sun.

$\boldsymbol{a}_i$ includes for example: satellites, general relativity, asteroids, the galaxy, nearby stars, passing stars and solar mass loss. In this work we neglected all the effects of $\boldsymbol{a}_i$ and other dissipative forces for the sake of simplicity. Note that equation (1) composes a Hamiltonian system only when we can derive $\boldsymbol{a}_i$ from a kind of potential. Consequently, our approximation of neglecting $\boldsymbol{a}_i$ reduces the system (1) into a conservative one.

2.2 Initial conditions

We list our major six numerical integrations for all nine planets and two other integrations for the outer five planets in Table 1. Initial planetary orbital elements are taken from the Development Ephemeris of JPL, DE245 (cf. Standish 1990), and listed in Table 2–4. The effect of the Moon is basically bunched together with the mass of the Earth: we placed a hypothetical celestial body with mass equal to the sum of the mass of the Earth and the Moon and whose position is at the baricentre of the Earth–Moon system. In one integration called N_{-3}, we simply neglected the Moon.

The pair (N_{+1}, N_{-1}) uses a common initial condition. The pair (N_{+2}, N_{-2}) also uses a common initial condition. These two initial conditions are slightly different. The relative difference in initial planetary positions and velocities between N_{+1} and N_{+2} (and also N_{-1} and N_{-2}) are tabulated in Table 3.

Table 1. Description of the long-term numerical integrations. The upper six are for all nine planets, and the lower two are for the outer five planets (from Jupiter to Pluto). T denotes the length of integration.

	Planets	Direction	T (yr)	Notes
N_{+1}	whole 9	future	5.0×10^9	Earth–Moon baricentre
N_{+2}	whole 9	future	5.0×10^9	Earth–Moon baricentre
N_{+3}	whole 9	future	4.2×10^9	Earth–Moon baricentre, increased Sun mass
N_{-1}	whole 9	past	3.9×10^9	Earth–Moon baricentre
N_{-2}	whole 9	past	4.1×10^9	Earth–Moon baricentre
N_{-3}	whole 9	past	4.1×10^9	Earth
F_+	outer 5	future	5.0×10^{10}	Sun incorporates the mass of the inner planets
F_-	outer 5	past	5.0×10^{10}	Sun incorporates the mass of the inner planets

© Royal Astronomical Society • Provided by the NASA Astrophysics Data System

2002MNRAS.336..483I

Table 2. Initial conditions of heliocentric planetary positions r_i and velocities v_i used in the integrations N_{+1}, N_{-1}, N_{+3}, N_{-3}, F_+ and F_-. r_3 and v_3 represents the position and velocity of Earth–Moon baricentre used in N_{+1}, N_{-1} and N_{+3}. r'_3 and v'_3 represents the position and velocity of Earth used in N_{-3}. The integrations F_+ and F_- use only r_5, v_5 to r_9, v_9. The Solar system invariable plane is taken as the xy-plane. The unit of the position is au and that of velocity is au d^{-1}.

	x	y	z
r_1	$-1.269\,180\,624\,092\,95 \times 10^{-1}$	$-4.477\,508\,198\,281\,78 \times 10^{-1}$	$-3.172\,814\,142\,021\,21 \times 10^{-2}$
v_1	$+2.145\,975\,482\,343\,09 \times 10^{-2}$	$-6.312\,659\,724\,381\,56 \times 10^{-3}$	$-1.979\,438\,134\,681\,18 \times 10^{-3}$
r_2	$-7.189\,382\,445\,936\,97 \times 10^{-1}$	$-3.683\,060\,280\,091\,61 \times 10^{-2}$	$+2.186\,214\,105\,039\,87 \times 10^{-2}$
v_2	$+9.190\,166\,373\,069\,85 \times 10^{-4}$	$-2.028\,720\,830\,376\,35 \times 10^{-2}$	$-4.712\,731\,882\,338\,86 \times 10^{-4}$
r_3	$-1.824\,663\,621\,223\,58 \times 10^{-1}$	$+9.662\,261\,297\,275\,45 \times 10^{-1}$	$+3.395\,76\,595\,144\,958 \times 10^{-3}$
v_3	$-1.717\,936\,036\,606\,89 \times 10^{-2}$	$-3.255\,497\,505\,688\,02 \times 10^{-3}$	$-4.781\,110\,245\,387\,70 \times 10^{-4}$
r'_3	$-1.824\,427\,321\,680\,04 \times 10^{-1}$	$+9.662\,486\,142\,727\,94 \times 10^{-1}$	$+3.393\,630\,838\,671\,48 \times 10^{-3}$
v'_3	$-1.718\,390\,537\,545\,36 \times 10^{-2}$	$-3.250\,392\,793\,790\,74 \times 10^{-3}$	$-4.781\,061\,995\,766\,76 \times 10^{-4}$
r_4	$+1.391\,194\,598\,677\,18 \times 10^{0}$	$-5.707\,247\,228\,184\,69 \times 10^{-3}$	$+1.958\,023\,006\,035\,16 \times 10^{-3}$
v_4	$+5.790\,115\,267\,804\,07 \times 10^{-4}$	$+1.518\,751\,558\,413\,43 \times 10^{-2}$	$+4.455\,675\,799\,439\,64 \times 10^{-4}$
r_5	$+3.986\,088\,540\,490\,54 \times 10^{0}$	$+2.960\,631\,490\,418\,22 \times 10^{0}$	$+2.779\,250\,439\,011\,18 \times 10^{-2}$
v_5	$-4.604\,437\,998\,175\,29 \times 10^{-3}$	$+6.417\,877\,688\,314\,58 \times 10^{-3}$	$+9.195\,113\,886\,976\,71 \times 10^{-6}$
r_6	$+6.377\,297\,171\,995\,65 \times 10^{0}$	$+6.606\,954\,603\,275\,79 \times 10^{0}$	$-1.459\,987\,734\,956\,59 \times 10^{-1}$
v_6	$-4.315\,113\,791\,005\,57 \times 10^{-3}$	$+3.866\,355\,851\,759\,66 \times 10^{-3}$	$+2.255\,490\,682\,460\,28 \times 10^{-5}$
r_7	$+1.450\,920\,250\,089\,10 \times 10^{1}$	$-1.365\,463\,701\,060\,73 \times 10^{1}$	$+2.667\,570\,613\,114\,20 \times 10^{-2}$
v_7	$+2.662\,948\,377\,580\,73 \times 10^{-3}$	$+2.687\,056\,727\,515\,16 \times 10^{-3}$	$+6.781\,620\,296\,113\,45 \times 10^{-5}$
r_8	$+1.694\,149\,604\,226\,77 \times 10^{1}$	$-2.490\,194\,581\,344\,67 \times 10^{1}$	$+3.607\,244\,966\,794\,61 \times 10^{-1}$
v_8	$+2.570\,995\,247\,934\,15 \times 10^{-3}$	$+1.791\,376\,414\,808\,37 \times 10^{-3}$	$-1.334\,389\,599\,420\,56 \times 10^{-5}$
r_9	$-9.869\,829\,401\,329\,05 \times 10^{0}$	$-2.805\,953\,708\,701\,44 \times 10^{1}$	$+5.356\,149\,276\,537\,37 \times 10^{0}$
v_9	$+3.054\,884\,779\,900\,26 \times 10^{-3}$	$-1.515\,512\,321\,044\,07 \times 10^{-3}$	$-6.451\,894\,168\,821\,79 \times 10^{-4}$

Table 3. Relative difference in initial of planetary positions and velocities between N_{+1} and N_{+2} (and also N_{-1} and N_{-2}). For example, $\delta r_{1x} = (r_{1x}^{N_{+1}} - r_{1x}^{N_{+2}})/r_{1x}^{N_{+1}} = (r_{1x}^{N_{-1}} - r_{1x}^{N_{-2}})/r_{1x}^{N_{-1}}$.

	x	y	z
δr_1	$+6.708\,2659 \times 10^{-5}$	$-1.976\,6372 \times 10^{-5}$	$-6.188\,6520 \times 10^{-6}$
δv_1	$+1.161\,9756 \times 10^{-6}$	$+4.092\,6775 \times 10^{-6}$	$+2.891\,5540 \times 10^{-7}$
δr_2	$+2.522\,6952 \times 10^{-9}$	$-4.872\,7168 \times 10^{-7}$	$-1.587\,4563 \times 10^{-8}$
δv_2	$+1.738\,0973 \times 10^{-8}$	$-5.012\,4943 \times 10^{-8}$	$-1.828\,0344 \times 10^{-9}$
δr_3	$-1.047\,1687 \times 10^{-6}$	$-1.702\,5629 \times 10^{-8}$	$+6.910\,1844 \times 10^{-8}$
δv_3	$-4.913\,9664 \times 10^{-8}$	$-4.773\,5453 \times 10^{-8}$	$-2.886\,7561 \times 10^{-9}$
δr_4	$-2.345\,2534 \times 10^{-6}$	$+2.701\,8727 \times 10^{-6}$	$+5.714\,6733 \times 10^{-8}$
δv_4	$-4.546\,7641 \times 10^{-8}$	$-5.552\,4810 \times 10^{-8}$	$-2.797\,5530 \times 10^{-9}$
δr_5	$-1.896\,4696 \times 10^{-6}$	$+2.762\,6629 \times 10^{-6}$	$+5.987\,4157 \times 10^{-8}$
δv_5	$-4.438\,2387 \times 10^{-6}$	$+6.066\,2085 \times 10^{-6}$	$+5.980\,6160 \times 10^{-9}$
δr_6	$+3.800\,3858 \times 10^{-3}$	$+2.826\,8716 \times 10^{-3}$	$+2.656\,7608 \times 10^{-5}$
δv_6	$-5.669\,1177 \times 10^{-6}$	$+7.168\,4120 \times 10^{-6}$	$+1.242\,2829 \times 10^{-8}$
δr_7	$+5.620\,1744 \times 10^{-3}$	$+4.712\,5183 \times 10^{-3}$	$-1.512\,4878 \times 10^{-5}$
δv_7	$-5.552\,7100 \times 10^{-6}$	$+7.285\,2927 \times 10^{-6}$	$+1.537\,6632 \times 10^{-8}$
δr_8	$+6.252\,6190 \times 10^{-3}$	$+4.116\,8841 \times 10^{-3}$	$-1.396\,0963 \times 10^{-5}$
δv_8	$-5.420\,1588 \times 10^{-6}$	$+7.377\,0756 \times 10^{-6}$	$+1.468\,9389 \times 10^{-8}$
δr_9	$+7.123\,8486 \times 10^{-3}$	$+2.835\,5964 \times 10^{-3}$	$+4.597\,6089 \times 10^{-6}$
δv_9	$-5.420\,1359 \times 10^{-6}$	$+7.377\,0646 \times 10^{-6}$	$+1.468\,4610 \times 10^{-8}$

Table 4. The mass of the Sun $M_\odot$ and the relative planetary masses used in the numerical integrations. m'_3 is only used in N_{-3}. The mass of the Sun which is greater than unity is used in F_+, F_- and N_{+3}.

$1/m_1$	6023 600.000 000 000	
$1/m_2$	408 523.710 000 0000	
$1/m'_3$	332 946.047 984 7735	only Earth (N_{-3})
$1/m_3$	328 900.560 000 0000	Earth + Moon
$1/m_4$	3098 708.000 000 007	
$1/m_5$	1047.348 599 999 995	
$1/m_6$	3497.897 999 999 658	
$1/m_7$	22 902.939 999 402 87	
$1/m_8$	19 412.240 000 261 45	
$1/m_9$	134 999 999.983 5724	
$M_\odot$	1.0	N_{+1}, N_{-1}, N_{+2}, N_{-2}, N_{-3}
	1.000 005 9401	N_{+3}, F_+, F_-

We also show the mass of the planets and the Sun in Table 4, which are also from DE245. We use the Gaussian unit system with the Gauss constant $k = \sqrt{G} = 0.017\,202\,098\,95$, in which the mass of the Sun is basically unity. In $F_\pm$ integrations, the mass of the Sun is slightly increased (from unity to 1.000 005 9401), owing to the incorporation of the mass of the inner four planets with that of the Sun. In addition, we use this increased mass of the Sun in N_{+3} to make a different initial condition than in other integrations.

The integration length of $\pm 5 \times 10^{10}$ yr for the integrations $F_\pm$ of the outer five planets seems to make no sense in practice, since the age of the Solar system is expected to be much less than the period. Note that our intention here is to show the very long-term stability of the outer Solar system as a typical example of point-mass dynamical systems, not to insist that the outer Solar system will really survive over this long interval.

We are now planning to integrate more detailed and realistic equations of motion of planets including the effects of the Moon and general relativity (cf. Quinn, Tremaine & Duncan 1991), using the Picard–Chebyshev numerical perturbation technique, which is well suited to vector integration (Fukushima 1997a,b).

2.3 Numerical method

We utilize a second-order Wisdom–Holman symplectic map as our main integration method (Wisdom & Holman 1991; Kinoshita, Yoshida & Nakai 1991) with a special start-up procedure to reduce

© Royal Astronomical Society • Provided by the NASA Astrophysics Data System

2002MNRAS.336..483I

the truncation error of angle variables, 'warm start' (Saha & Tremaine 1992, 1994).

The stepsize for the numerical integrations is 8 d throughout all integrations of the nine planets ($N_{\pm1,2,3}$), which is about 1/11 of the orbital period of the innermost planet (Mercury). As for the determination of stepsize, we partly follow the previous numerical integration of all nine planets in Sussman & Wisdom (1988, 7.2 d) and Saha & Tremaine (1994, 225/32 d). We rounded the decimal part of the their stepsizes to 8 to make the stepsize a multiple of 2 in order to reduce the accumulation of round-off error in the computation processes. In relation to this, Wisdom & Holman (1991) performed numerical integrations of the outer five planetary orbits using the symplectic map with a stepsize of 400 d, 1/10.83 of the orbital period of Jupiter. Their result seems to be accurate enough, which partly justifies our method of determining the stepsize. However, since the eccentricity of Jupiter (∼0.05) is much smaller than that of Mercury (∼0.2), we need some care when we compare these integrations simply in terms of stepsizes.

In the integration of the outer five planets ($F_{\pm}$), we fixed the stepsize at 400 d.

We adopt Gauss' f and g functions in the symplectic map together with the third-order Halley method (Danby 1992) as a solver for Kepler equations. The number of maximum iterations we set in Halley's method is 15, but they never reached the maximum in any of our integrations.

The interval of the data output is 200 000 d (∼547 yr) for the calculations of all nine planets ($N_{\pm1,2,3}$), and about 8000 000 d (∼21 903 yr) for the integration of the outer five planets ($F_{\pm}$).

Although no output filtering was done when the numerical integrations were in process, we applied a low-pass filter to the raw orbital data after we had completed all the calculations. See Section 4.1 for more detail.

2.4 Error estimation

2.4.1 *Relative errors in total energy and angular momentum*

According to one of the basic properties of symplectic integrators, which conserve the physically conservative quantities well (total orbital energy and angular momentum), our long-term numerical integrations seem to have been performed with very small errors. The averaged relative errors of total energy ($\sim10^{-9}$) and of total angular momentum ($\sim10^{-11}$) have remained nearly constant throughout the integration period (Fig. 1). The special startup procedure, warm start, would have reduced the averaged relative error in total energy by about one order of magnitude or more.

Note that different operating systems, different mathematical libraries, and different hardware architectures result in different numerical errors, through the variations in round-off error handling and numerical algorithms. In the upper panel of Fig. 1, we can recognize this situation in the secular numerical error in the total angular momentum, which should be rigorously preserved up to machine-ϵ precision.

2.4.2 *Error in planetary longitudes*

Since the symplectic maps preserve total energy and total angular momentum of N-body dynamical systems inherently well, the degree of their preservation may not be a good measure of the accuracy of numerical integrations, especially as a measure of the positional error of planets, i.e. the error in planetary longitudes. To estimate the numerical error in the planetary longitudes, we performed the following procedures. We compared the result of our main long-term integrations with some test integrations, which span much shorter periods but with much higher accuracy than the main integrations. For this purpose, we performed a much more accurate integration with a stepsize of 0.125 d (1/64 of the main integrations) spanning 3×10^5 yr, starting with the same initial conditions as in the N_{-1} integration. We consider that this test integration provides us with a 'pseudo-true' solution of planetary orbital evolution. Next, we compare the test integration with the main integration, N_{-1}. For the period of 3×10^5 yr, we see a difference in mean anomalies of the Earth between the two integrations of ∼0.52° (in the case of the N_{-1} integration). This difference can be extrapolated to the value ∼8700°, about 25 rotations of Earth after 5 Gyr, since the error of longitudes increases linearly with time in the symplectic map. Similarly, the longitude error of Pluto can be estimated as ∼12°. This value for Pluto is much better than the result in Kinoshita & Nakai (1996) where the difference is estimated as ∼60°.

3 NUMERICAL RESULTS – I. GLANCE AT THE RAW DATA

In this section we briefly review the long-term stability of planetary orbital motion through some snapshots of raw numerical data. The orbital motion of planets indicates long-term stability in all of our numerical integrations: no orbital crossings nor close encounters between any pair of planets took place.

3.1 General description of the stability of planetary orbits

First, we briefly look at the general character of the long-term stability of planetary orbits. Our interest here focuses particularly on the inner four terrestrial planets for which the orbital time-scales are much shorter than those of the outer five planets. As we can see clearly from the planar orbital configurations shown in Figs 2 and 3, orbital positions of the terrestrial planets differ little between the initial and final part of each numerical integration, which spans several Gyr. The solid lines denoting the present orbits of the planets lie almost within the swarm of dots even in the final part of integrations (b) and (d). This indicates that throughout the entire integration period the almost regular variations of planetary orbital motion remain nearly the same as they are at present.

The variation of eccentricities and orbital inclinations for the inner four planets in the initial and final part of the integration N_{+1} is shown in Fig. 4. As expected, the character of the variation of planetary orbital elements does not differ significantly between the initial and final part of each integration, at least for Venus, Earth and Mars. The elements of Mercury, especially its eccentricity, seem to change to a significant extent. This is partly because the orbital time-scale of the planet is the shortest of all the planets, which leads to a more rapid orbital evolution than other planets; the innermost planet may be nearest to instability. This result appears to be in some agreement with Laskar's (1994, 1996) expectations that large and irregular variations appear in the eccentricities and inclinations of Mercury on a time-scale of several 10^9 yr. However, the effect of the possible instability of the orbit of Mercury may not fatally affect the global stability of the whole planetary system owing to the small mass of Mercury. We will mention briefly the long-term orbital evolution of Mercury later in Section 4 using low-pass filtered orbital elements.

The orbital motion of the outer five planets seems rigorously stable and quite regular over this time-span (see also Section 5).

© Royal Astronomical Society • Provided by the NASA Astrophysics Data System

2002MNRAS.336..483I

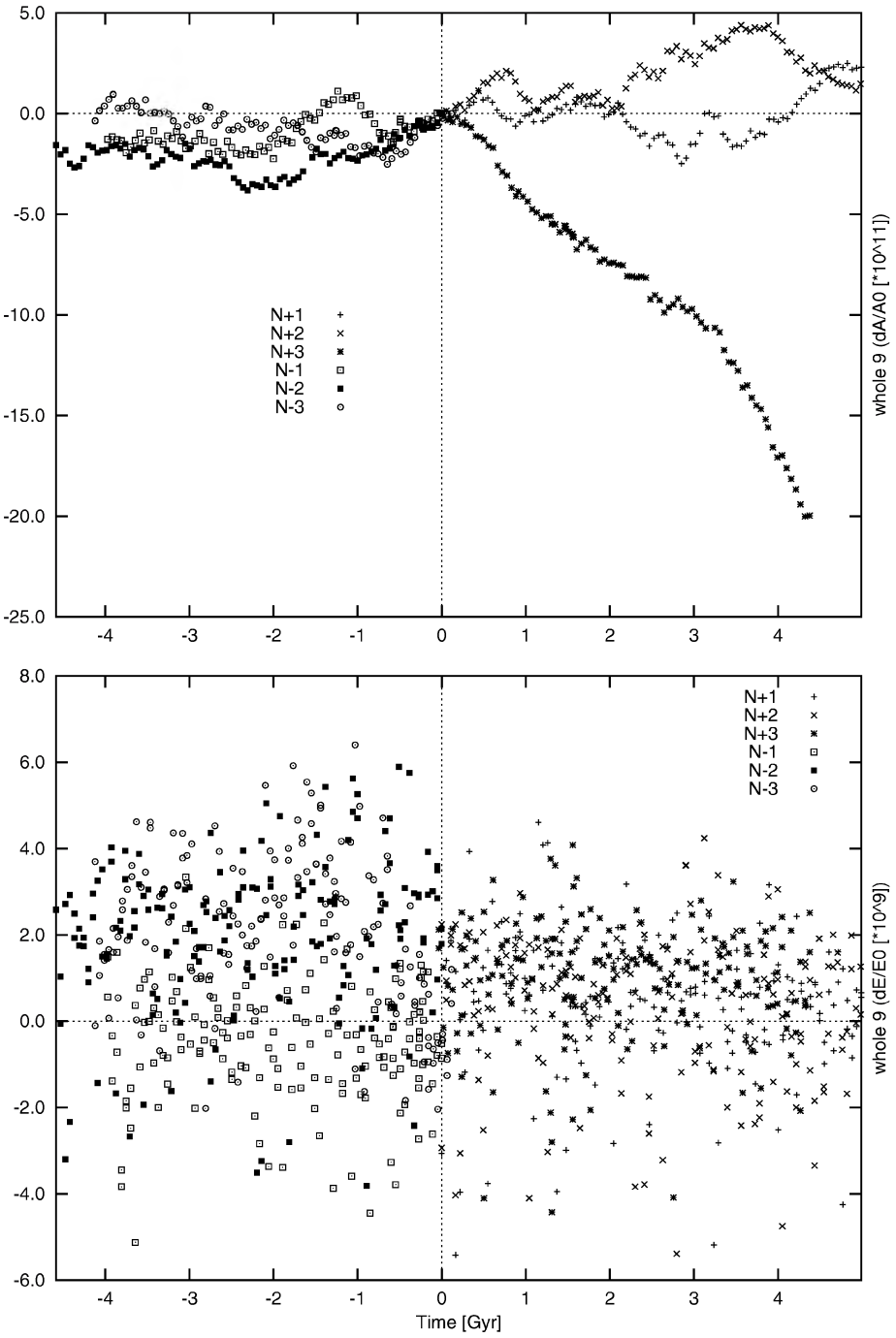

Figure 1. Relative numerical error of the total angular momentum $\delta A/A_0$ and the total energy $\delta E/E_0$ in our numerical integrations $N_{\pm 1,2,3}$, where δE and δA are the absolute change of the total energy and total angular momentum, respectively, and E_0 and A_0 are their initial values. The horizontal unit is Gyr.

3.2 Time–frequency maps

Although the planetary motion exhibits very long-term stability defined as the non-existence of close encounter events, the chaotic nature of planetary dynamics can change the oscillatory period and amplitude of planetary orbital motion gradually over such long timespans. Even such slight fluctuations of orbital variation in the frequency domain, particularly in the case of Earth, can potentially have a significant effect on its surface climate system through solar insolation variation (cf. Berger 1988).

To give an overview of the long-term change in periodicity in planetary orbital motion, we performed many fast Fourier transformations (FFTs) along the time axis, and superposed the resulting periodgrams to draw two-dimensional time–frequency maps. The

© Royal Astronomical Society • Provided by the NASA Astrophysics Data System

2002MNRAS.336..483I

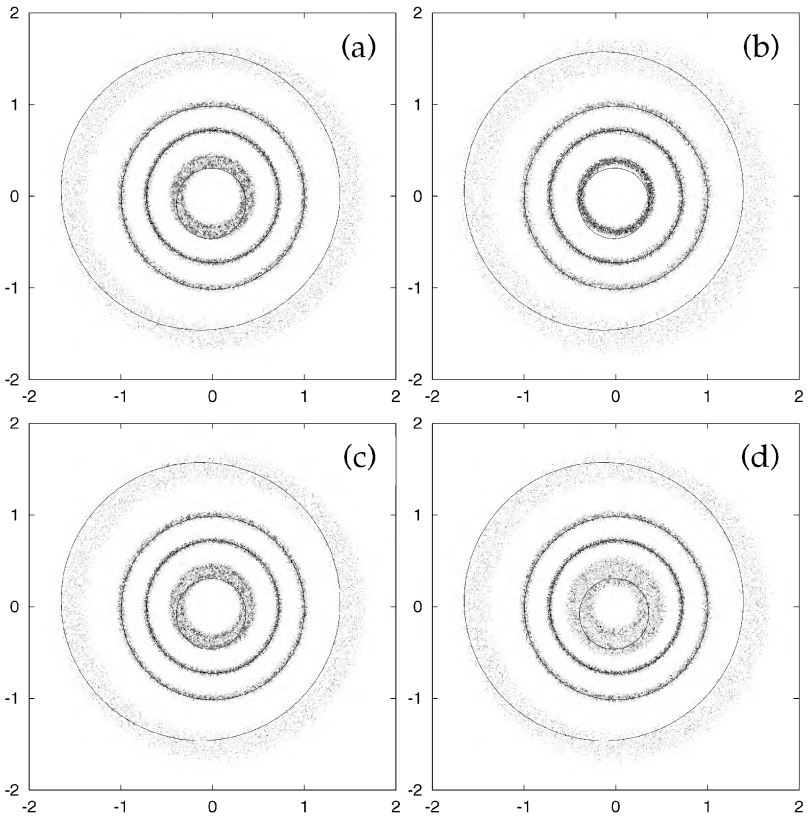

Figure 2. Vertical view of the four inner planetary orbits (from the z-axis direction) at the initial and final parts of the integrations $N_{\pm 1}$. The axes units are au. The xy-plane is set to the invariant plane of Solar system total angular momentum. (a) The initial part of N_{+1} ($t = 0$ to 0.0547×10^9 yr). (b) The final part of N_{+1} ($t = 4.9339 \times 10^8$ to 4.9886×10^9 yr). (c) The initial part of N_{-1} ($t = 0$ to -0.0547×10^9 yr). (d) The final part of N_{-1} ($t = -3.9180 \times 10^9$ to -3.9727×10^9 yr). In each panel, a total of 23 684 points are plotted with an interval of about 2190 yr over 5.47×10^7 yr. Solid lines in each panel denote the present orbits of the four terrestrial planets (taken from DE245).

specific approach to drawing these time–frequency maps in this paper is very simple – much simpler than the wavelet analysis or Laskar's (1990, 1993) frequency analysis.

(i) Divide the low-pass filtered orbital data into many fragments of the same length. The length of each data segment should be a multiple of 2 in order to apply the FFT.

(ii) Each fragment of the data has a large overlapping part: for example, when the ith data begins from $t = t_i$ and ends at $t = t_i + T$, the next data segment ranges from $t_i + \delta T \leqslant t_i + \delta T + T$, where $\delta T \ll T$. We continue this division until we reach a certain number N by which $t_n + T$ reaches the total integration length.

(iii) We apply an FFT to each of the data fragments, and obtain n frequency diagrams.

(iv) In each frequency diagram obtained above, the strength of periodicity can be replaced by a grey-scale (or colour) chart.

(v) We perform the replacement, and connect all the grey-scale (or colour) charts into one graph for each integration. The horizontal axis of these new graphs should be the time, i.e. the starting times of each fragment of data (t_i, where $i = 1, \ldots, n$). The vertical axis represents the period (or frequency) of the oscillation of orbital elements.

We have adopted an FFT because of its overwhelming speed, since the amount of numerical data to be decomposed into frequency components is terribly huge (several tens of Gbytes).

A typical example of the time–frequency map created by the above procedures is shown in a grey-scale diagram as Fig. 5, which shows the variation of periodicity in the eccentricity and inclination of Earth in N_{+2} integration. In Fig. 5, the dark area shows that at the time indicated by the value on the abscissa, the periodicity indicated by the ordinate is stronger than in the lighter area around it. We can recognize from this map that the periodicity of the eccentricity and inclination of Earth only changes slightly over the entire period covered by the N_{+2} integration. This nearly regular trend is qualitatively the same in other integrations and for other planets, although typical frequencies differ planet by planet and element by element.

4 NUMERICAL RESULTS – II. LOW-FREQUENCY ORBITAL VARIATION

4.1 Low-pass filtering

Long-term variations of planetary orbital elements are, in a sense, likely to be buried in short periodic oscillations in raw numerical output. We wanted to remove the short periodic oscillations in some way and extract long-periodic or, if any, secular components buried in the raw numerical data. For this purpose, we applied a low-pass filter to the raw orbital elements. The specifications of the low-pass filter are listed in Table 5. When we denote the filter coefficients as

© Royal Astronomical Society • Provided by the NASA Astrophysics Data System

2002MNRAS.336..483I

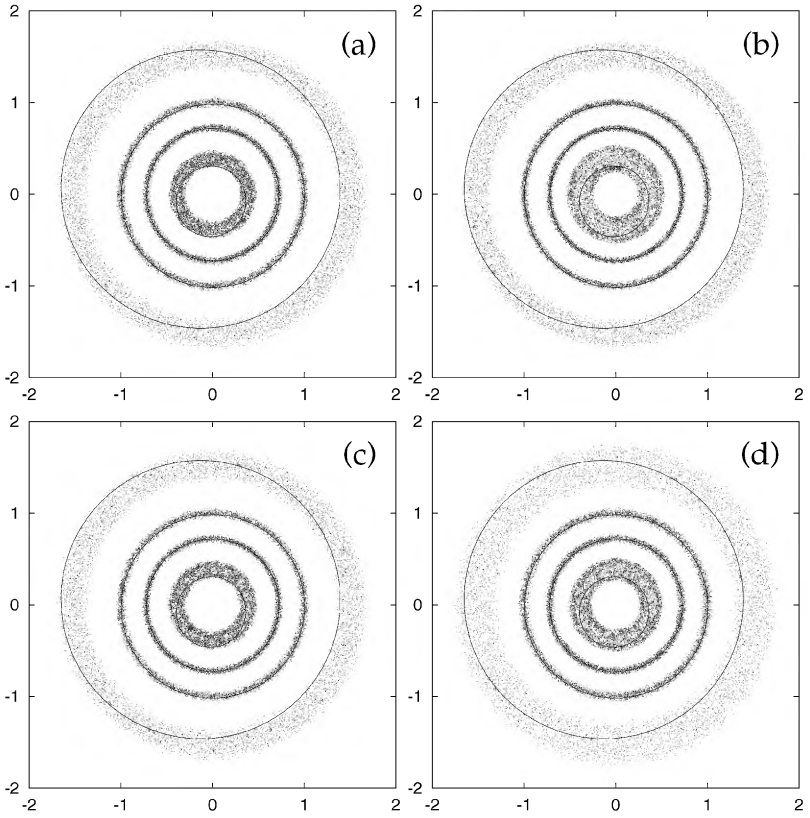

Figure 3. Same as in Fig. 2, but for $N_{\pm 2}$. (a) The initial part of N_{+2} ($t = 0$ to 0.0547×10^9 yr). (b) The final part of N_{+2} ($t = 4.9829 \times 10^8$ to 5.0376×10^9 yr). (c) The initial part of N_{-2} ($t = 0$ to -0.0547×10^9 yr). (d) The final part of N_{-2} ($t = -3.9726 \times 10^9$ to -3.9179×10^9 yr).

h_j ($j = 0, \ldots, \mathcal{M}$), input data x_i and output data y_i are related as (Oppenheim, Schafer & Buck 1999)

$$y_i = \sum_{j=0}^{\mathcal{M}} h_j x_{i-j}, \tag{2}$$

where $\mathcal{M}$ is the degree of the filter. The filter coefficients in the frequency and the time domain are displayed in Fig. 6.

4.2 Long-term exchange of orbital energy and angular momentum

We calculate very long-periodic variation and exchange of planetary orbital energy and angular momentum using filtered Delaunay elements L, G, H. G and H are equivalent to the planetary orbital angular momentum and its vertical component per unit mass. L is related to the planetary orbital energy E per unit mass as $E = -\mu^2/2L^2$. If the system is completely linear, the orbital energy and the angular momentum in each frequency bin must be constant. Non-linearity in the planetary system can cause an exchange of energy and angular momentum in the frequency domain. The amplitude of the lowest-frequency oscillation should increase if the system is unstable and breaks down gradually. However, such a symptom of instability is not prominent in our long-term integrations.

In Fig. 7, the total orbital energy and angular momentum of the four inner planets and all nine planets are shown for integration N_{+2}. The upper three panels show the long-periodic variation of total energy (denoted as E-E0), total angular momentum (G-G0), and the vertical component (H-H0) of the inner four planets calculated from the low-pass filtered Delaunay elements. E0, G0, H0 denote the initial values of each quantity. The absolute difference from the initial values is plotted in the panels. The lower three panels in each figure show E-E0, G-G0 and H-H0 of the total of nine planets. The fluctuation shown in the lower panels is virtually entirely a result of the massive jovian planets.

Comparing the variations of energy and angular momentum of the inner four planets and all nine planets, it is apparent that the amplitudes of those of the inner planets are much smaller than those of all nine planets: the amplitudes of the outer five planets are much larger than those of the inner planets. This does not mean that the inner terrestrial planetary subsystem is more stable than the outer one: this is simply a result of the relative smallness of the masses of the four terrestrial planets compared with those of the outer jovian planets. Another thing we notice is that the inner planetary subsystem may become unstable more rapidly than the outer one because of its shorter orbital time-scales. This can be seen in the panels denoted as inner 4 in Fig. 7 where the longer-periodic and irregular oscillations are more apparent than in the panels denoted as total 9. Actually, the fluctuations in the inner 4 panels are to a large extent as a result of the orbital variation of the Mercury. However, we cannot neglect the contribution from other terrestrial planets, as we will see in subsequent sections.

4.3 Conservation and variation of the angular momentum deficit

Among many indicators of planetary orbital stability and long-term evolution, the angular momentum deficit (AMD) is one of the most

© Royal Astronomical Society • Provided by the NASA Astrophysics Data System

2002MNRAS.336..483I

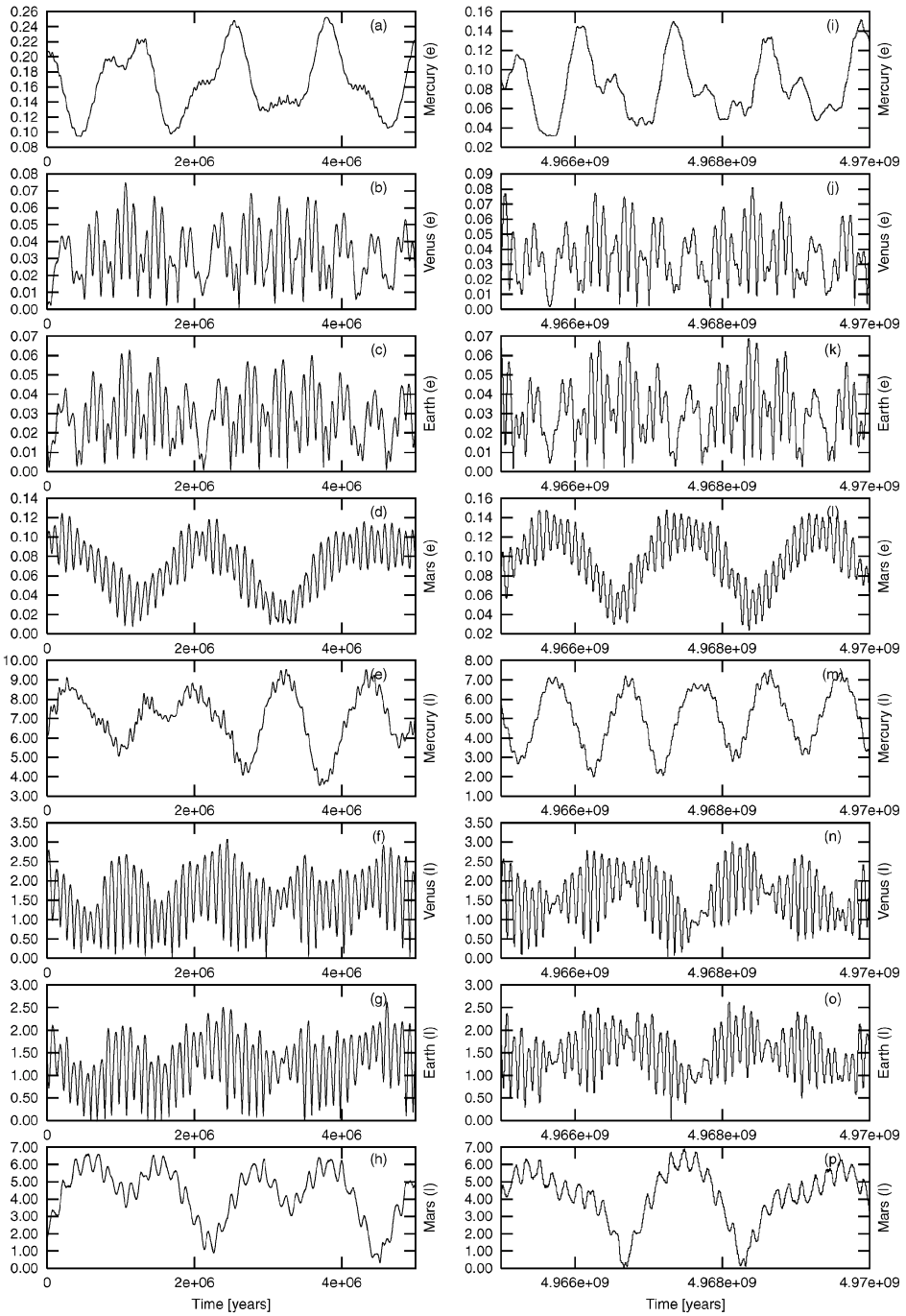

Figure 4. Eccentricities and inclinations of the four inner planetary orbits in the initial and final parts of the integration N_{+1}. (a)–(d) Eccentricities of Mercury, Venus, Earth and Mars at the beginning of the integration. (e)–(h) Inclinations of Mercury, Venus, Earth and Mars at the beginning of the integration. (i)–(l) Eccentricities of Mercury, Venus, Earth and Mars at the end of the integration. (m)–(p) Inclinations of Mercury, Venus, Earth and Mars at the end of the integration. All the elements are reckoned on the Solar system invariable plane with a heliocentric origin. The unit of inclination is the degree.

interesting quantities. When we consider the z-axis component C of the total angular momentum of system as

$$C = \sum_{j=1}^{N} \frac{m_j \, \mathrm{M}_\odot}{m_j + \mathrm{M}_\odot} \sqrt{\mu_j a_j} \sqrt{1 - e_j^2} \cos I_j, \tag{3}$$

where

$$\mu_j = G\left(\mathrm{M}_\odot + m_j\right), \tag{4}$$

C should be conserved exactly, AMD C' is defined as below:

$$C' = \sum_{j=1}^{N} \frac{m_j \, \mathrm{M}_\odot}{m_j + \mathrm{M}_\odot} \sqrt{\mu_j a_j} \left(1 - \sqrt{1 - e_j^2} \cos I_j\right). \tag{5}$$

The AMD has a dynamical meaning that indicates the deviation of planetary orbits from planar and circular motion: if $e_j = I_j = 0$ for all j, then $C' = 0$. Laskar (1997) remarked that the AMD C' itself

© Royal Astronomical Society • Provided by the NASA Astrophysics Data System

2002MNRAS.336..483I

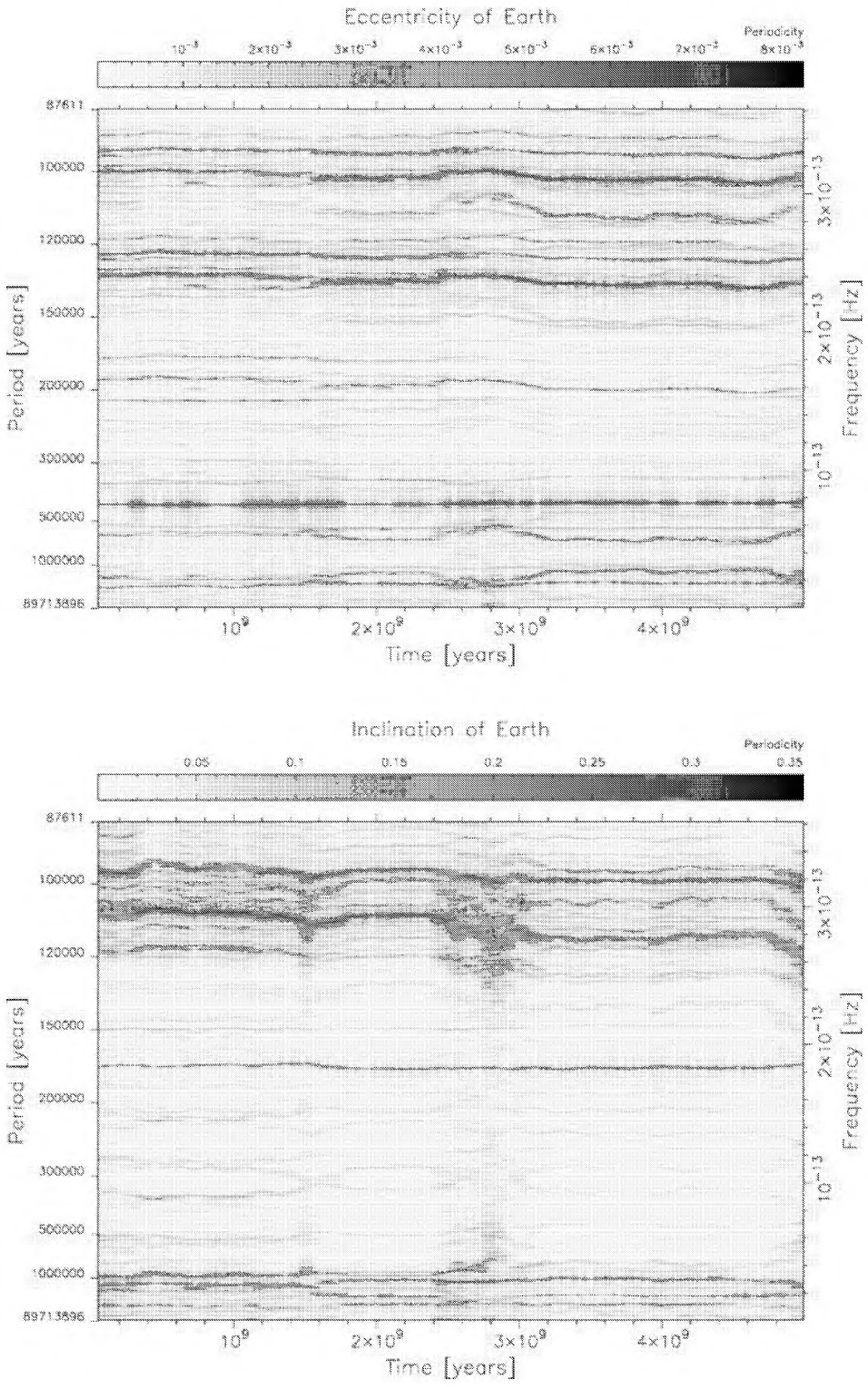

Figure 5. Time–frequency map for the e and I of the Earth in N_{+2} series.

is also conserved besides C in averaged equations of motion, and suggested that the conservation of AMD is one of the key ingredients that determines the spacing of the four inner planets (Laskar 1997, 2000).

The AMD of the inner four planets is not conserved because of the perturbation from outer giant planets. However, since the orbital motion of the outer planets is quite regular, the AMD of the inner four planets, C'', may be expected to be roughly constant.

© Royal Astronomical Society • Provided by the NASA Astrophysics Data System

2002MNRAS.336..483I

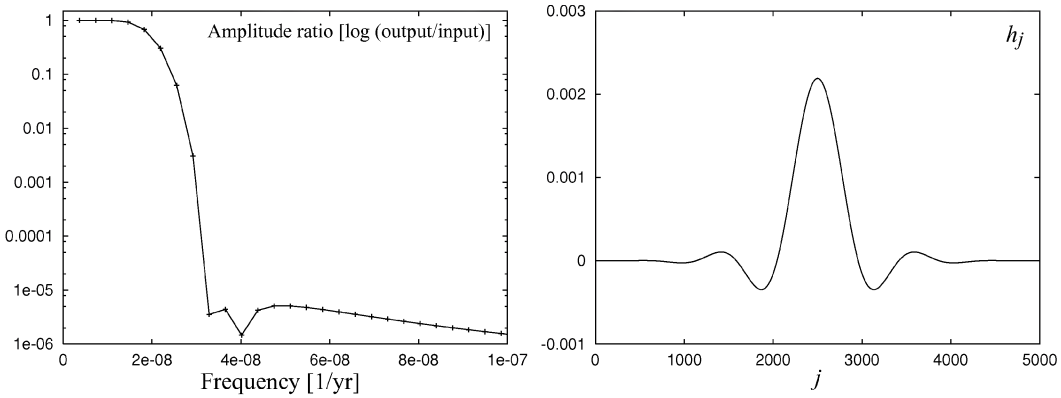

Figure 6. Frequency domain (left) and time domain (right) characteristics of the low-pass filter. Cut-off period $\sim 5 \times 10^7$ yr. The filter length is $5001 \times \mathrm{d}t$ where $\mathrm{d}t$ is the step-interval of the original data (i.e. $\mathrm{d}t = 2 \times 10^6$ d).

Table 5. Specification of the low-pass filter.

Cut-off period	5×10^7 yr
Degree of filter (M)	5001
Filter length	$\sim 2.74 \times 10^8$ yr
Worst reduction ratio	100 dB

$$C'' = \sum_{j=1}^{4} \frac{m_j\,\mathrm{M}_\odot}{m_j + \mathrm{M}_\odot} \sqrt{\mu_j a_j}\left(1 - \sqrt{1 - e_j^2}\cos I_j\right). \tag{6}$$

We have plotted C'' and the AMD of each inner planet in Fig. 8 for each integration. What we notice first is that the variation of C'' is mostly driven by the variation of the AMD of Mercury. The variational amplitude of the AMD of Mercury is much larger than that of the total AMD of the other three inner planets ('V + E + M' in Fig. 8). This fact is directly connected to the relatively larger scale variation of the eccentricity and inclination of Mercury. As an example, in Fig. 9 we show the low-pass filtered eccentricity of Mercury in each integration. The behaviour of the eccentricity of Mercury in our integrations is qualitatively similar to the results from Laskar's secular perturbation theory (e.g. $e_{\max} \sim 0.35$ during $\sim \pm 4$ Gyr). However, it has no apparent secular increase that directly relates to the instability of the orbit of the planet.

Incidentally, it is rather curious that in the N_{+3} integration, the variational amplitudes of both the AMD and the eccentricity of Mercury are smaller than in other integrations. The only major difference of this N_{+3} integration from others is that we have increased the mass of the Sun by $\sim 6 \times 10^{-6}$ as in Table 4. It might be very interesting if such a slight increase of central mass were found to affect the overall stability of long-term planetary motion. We have to accumulate many more integrations from various different initial conditions to confirm whether this phenomenon is general or not.

4.4 Long-term coupling of several neighbouring planet pairs

Let us see some individual variations of planetary orbital energy and angular momentum expressed by the low-pass filtered Delaunay elements. Figs 10 and 11 show long-term evolution of the orbital energy of each planet and the angular momentum in N_{+1} and N_{-2} integrations. We notice that some planets form apparent pairs in terms of orbital energy and angular momentum exchange. In particular, Venus and Earth make a typical pair. In the figures, they show negative correlations in exchange of energy and positive correlations in exchange of angular momentum. The negative correlation in exchange of orbital energy means that the two planets form a closed dynamical system in terms of the orbital energy. The positive correlation in exchange of angular momentum means that the two planets are simultaneously under certain long-term perturbations. Candidates for perturbers are Jupiter and Saturn. Also in Fig. 11, we can see that Mars shows a positive correlation in the angular momentum variation to the Venus–Earth system. Mercury exhibits certain negative correlations in the angular momentum versus the Venus–Earth system, which seems to be a reaction caused by the conservation of angular momentum in the terrestrial planetary subsystem.

It is not clear at the moment why the Venus–Earth pair exhibits a negative correlation in energy exchange and a positive correlation in angular momentum exchange. We may possibly explain this through observing the general fact that there are no secular terms in planetary semimajor axes up to second-order perturbation theories (cf. Brouwer & Clemence 1961; Boccaletti & Pucacco 1998). This means that the planetary orbital energy (which is directly related to the semimajor axis a) might be much less affected by perturbing planets than is the angular momentum exchange (which relates to e). Hence, the eccentricities of Venus and Earth can be disturbed easily by Jupiter and Saturn, which results in a positive correlation in the angular momentum exchange. On the other hand, the semimajor axes of Venus and Earth are less likely to be disturbed by the jovian planets. Thus the energy exchange may be limited only within the Venus–Earth pair, which results in a negative correlation in the exchange of orbital energy in the pair.

As for the outer jovian planetary subsystem, Jupiter–Saturn and Uranus–Neptune seem to make dynamical pairs. However, the strength of their coupling is not as strong compared with that of the Venus–Earth pair.

5 $\pm 5 \times 10^{10}$-YR INTEGRATIONS OF OUTER PLANETARY ORBITS

Since the jovian planetary masses are much larger than the terrestrial planetary masses, we treat the jovian planetary system as an independent planetary system in terms of the study of its dynamical stability. Hence, we added a couple of trial integrations that span $\pm 5 \times 10^{10}$ yr, including only the outer five planets (the four jovian planets plus Pluto). The results exhibit the rigorous stability of the outer planetary system over this long time-span. Orbital configurations

© Royal Astronomical Society • Provided by the NASA Astrophysics Data System

2002MNRAS.336..483I

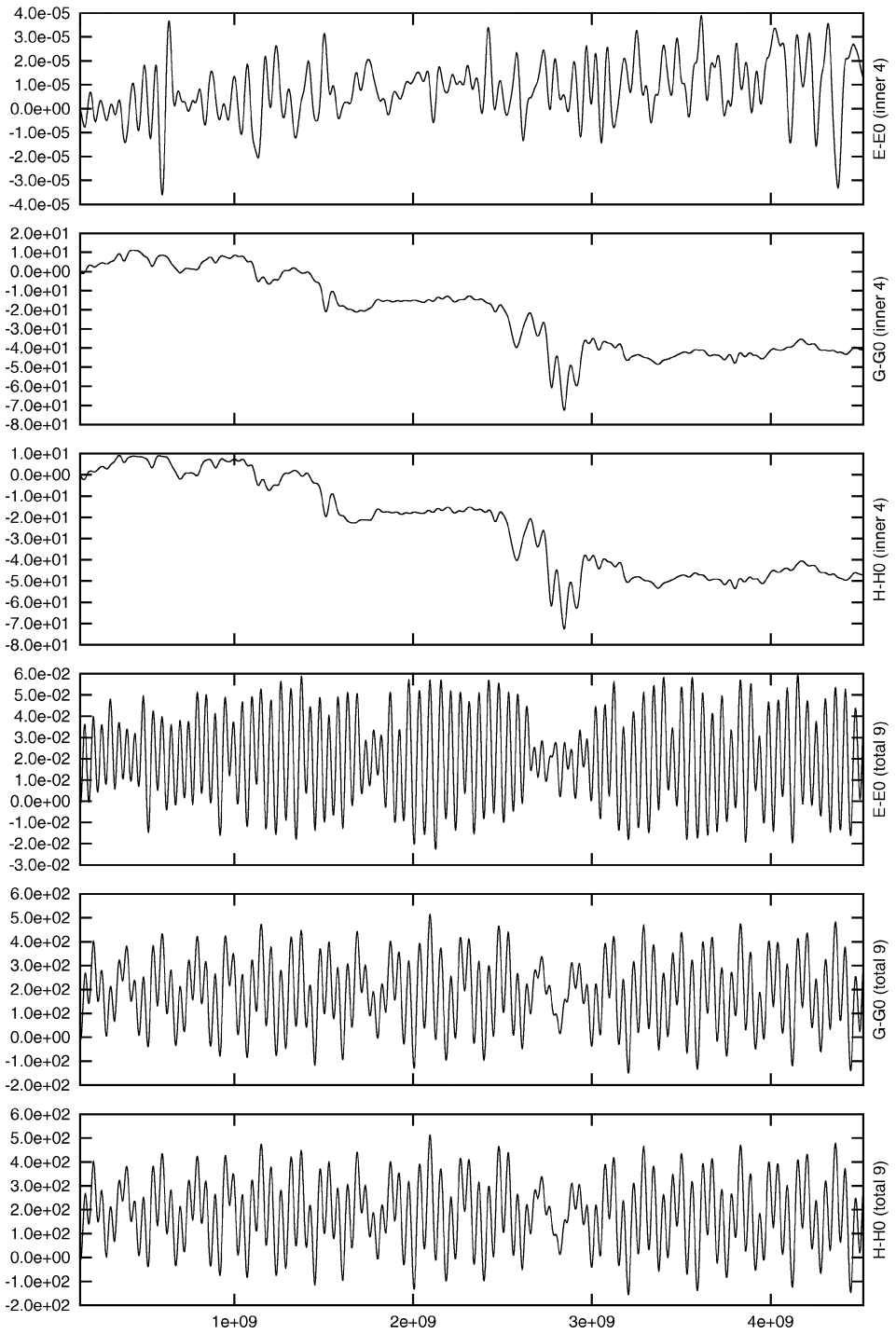

Figure 7. Absolute difference in total energy ($E - E_0$), angular momentum ($G - G_0$) and its vertical component ($H - H_0$) calculated by the low-pass filtered orbital elements in N_{+2} series. E is calculated from one of the Delaunay elements L as $E = -\mu^2/2L^2$. The upper three panels are for the inner four planets, and the lower three panels are for the total of nine planets. The unit of energy is 10^{-12} $M_\odot$ au^2 d^{-2}, and that of angular momentum is 10^{-12} $M_\odot$ au^2 d^{-1}. The unit of the horizontal axis is yr.

(Fig. 12), and variation of eccentricities and inclinations (Fig. 13) show this very long-term stability of the outer five planets in both the time and the frequency domains. Although we do not show maps here, the typical frequency of the orbital oscillation of Pluto and the other outer planets is almost constant during these very long-term integration periods, which is demonstrated in the time–frequency maps on our webpage.

In these two integrations, the relative numerical error in the total energy was $\sim 10^{-6}$ and that of the total angular momentum was $\sim 10^{-10}$.

© Royal Astronomical Society • Provided by the NASA Astrophysics Data System

2002MNRAS.336..483I

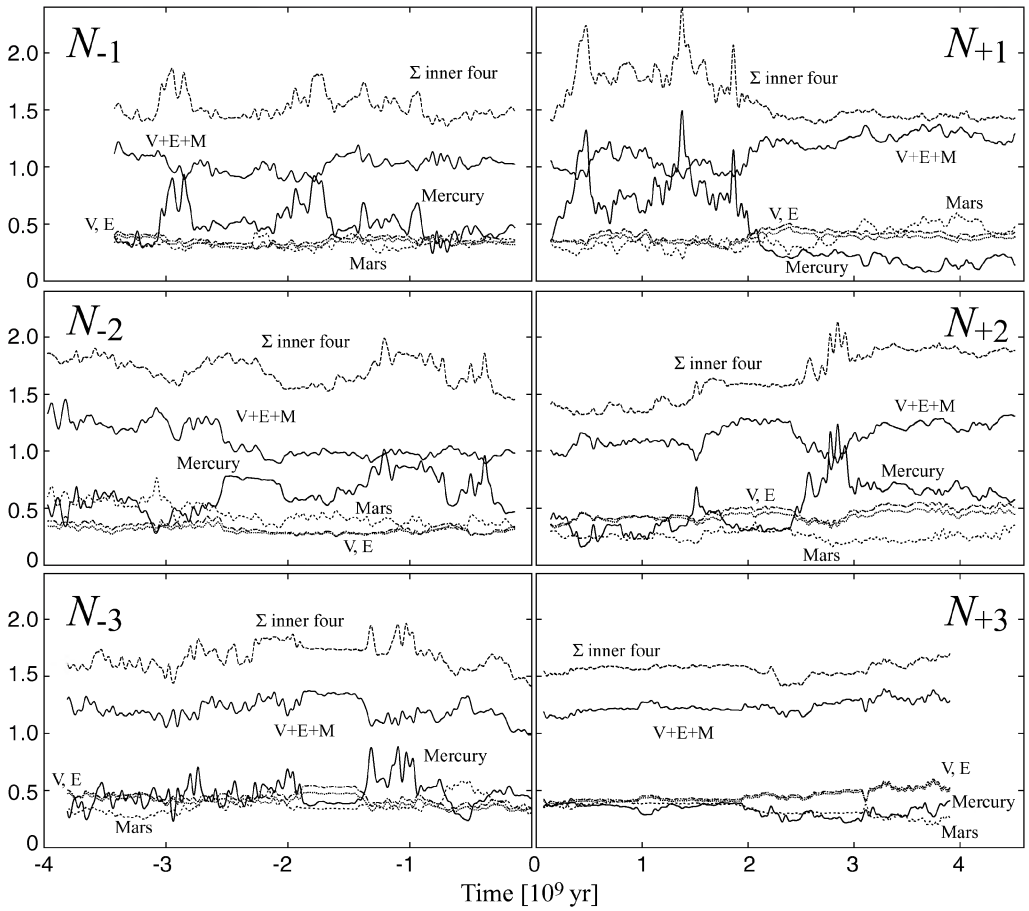

Figure 8. Angular momentum deficit of the inner four planets in each of our numerical integrations ($N_{\pm1,2,3}$). '$\sum$ inner four' denotes the total AMD of the inner four planets, 'V + E + M' denotes the total AMD of Venus, Earth and Mars. 'V' and 'E' denote the AMD of Venus and Earth, which are too similar to distinguish. The AMD of Mercury and Mars are also denoted as a thick solid line and a thin dotted line with labels 'Mercury' and 'Mars'. The unit of AMD is the same as that of the angular momentum in Gaussian units, i.e. 10^{-12} $M_\odot$ au^2 d^{-1}.

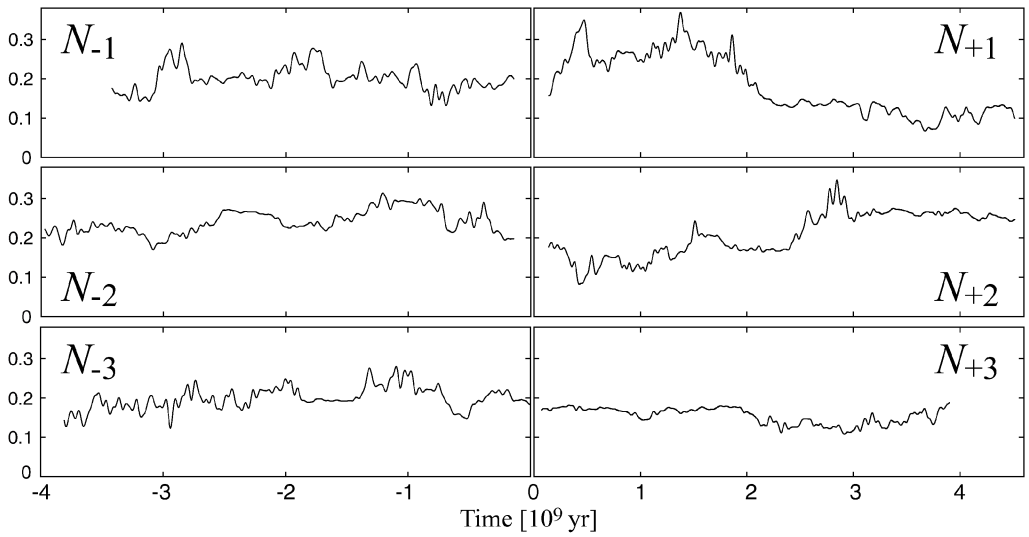

Figure 9. Low-pass filtered variation of the eccentricity of Mercury in each of our numerical integration ($N_{\pm1,2,3}$).

© Royal Astronomical Society • Provided by the NASA Astrophysics Data System

2002MNRAS.336..483I

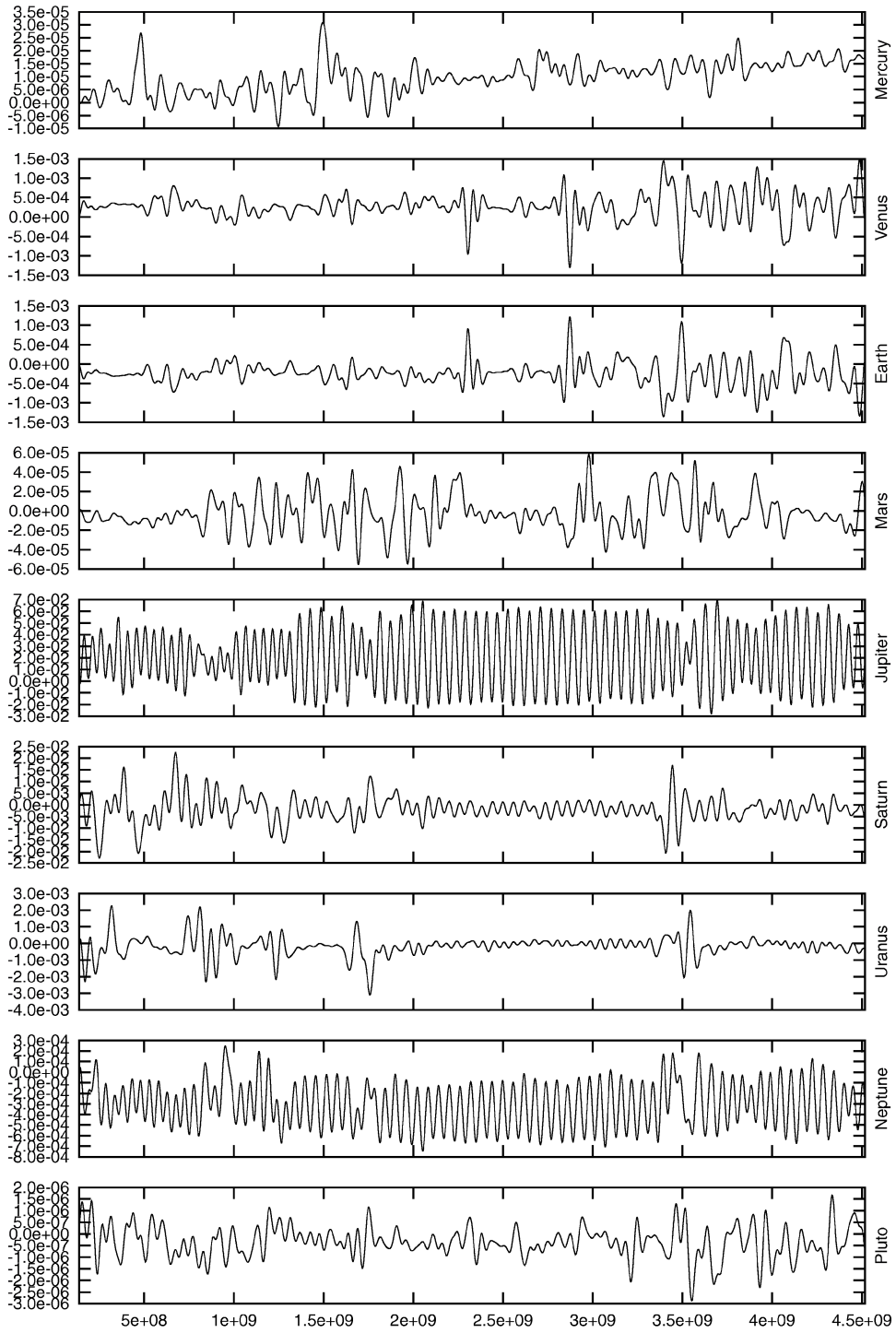

Figure 10. Variation of the orbital energy (absolute difference from the initial value) of each planet calculated from the Delaunay element, $L - L_0$, in N_{+1} series. The unit of the vertical axis is 10^{-12} $M_\odot$ au^2 d^{-2}. The unit of the horizontal axis is yr.

5.1 Resonances in the Neptune–Pluto system

Kinoshita & Nakai (1996) integrated the outer five planetary orbits over $\pm 5.5 \times 10^9$ yr. They found that four major resonances between Neptune and Pluto are maintained during the whole integration period, and that the resonances may be the main causes of the stability of the orbit of Pluto. The major four resonances found in previous research are as follows. In the following description, λ denotes the mean longitude, Ω is the longitude of the ascending node and ϖ is the longitude of perihelion. Subscripts P and N denote Pluto and Neptune.

(i) Mean motion resonance between Neptune and Pluto (3:2). The critical argument $\theta_1 = 3\lambda_P - 2\lambda_N - \varpi_P$ librates around 180°

© Royal Astronomical Society • Provided by the NASA Astrophysics Data System

2002MNRAS.336..483I

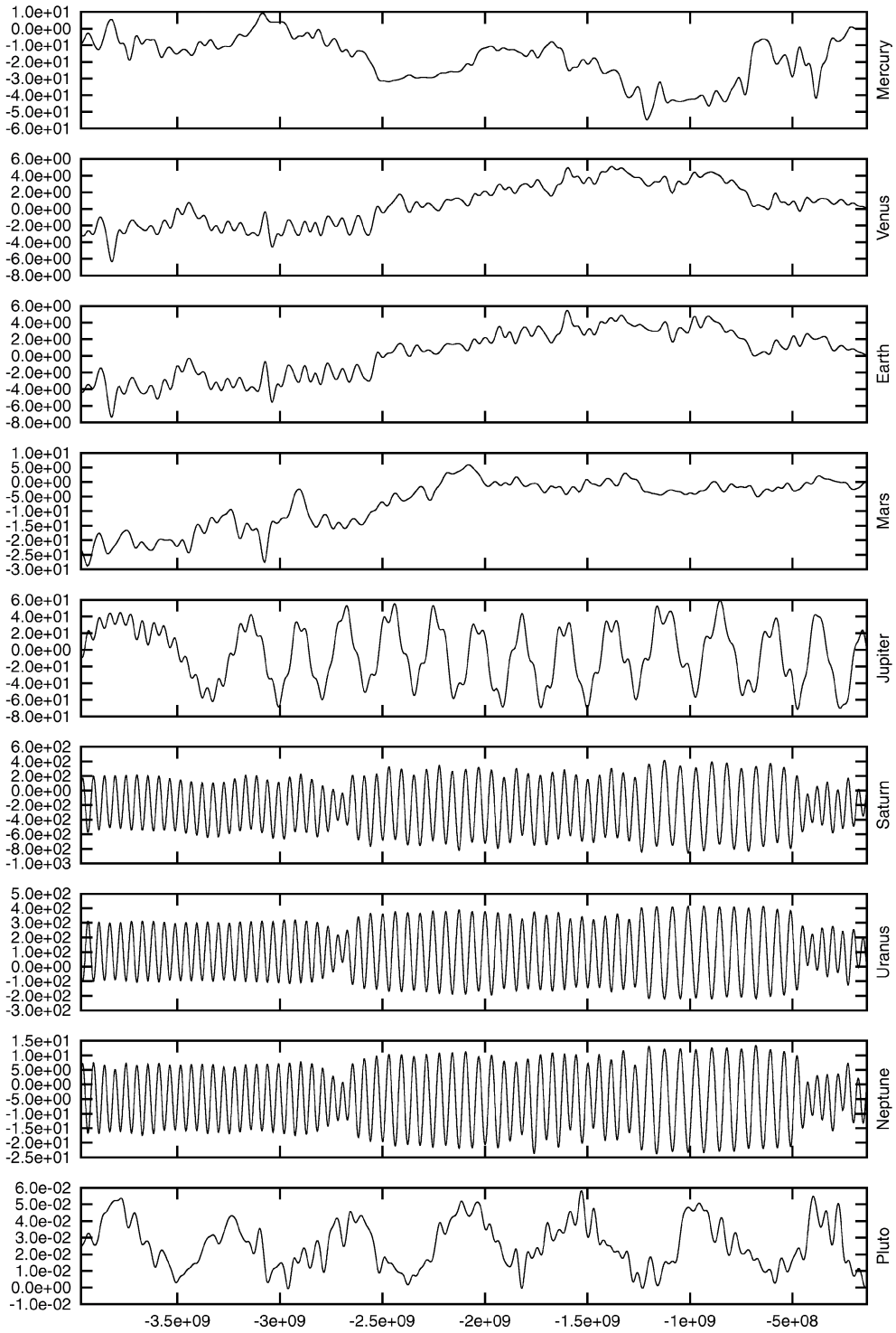

Figure 11. Variation of the orbital angular momentum (absolute difference from the initial value) of each planet calculated from the Delaunay element, $G - G_0$, in N_{-2} series. The unit of the vertical axis is 10^{-12} $M_\odot$ au^2 d^{-1}. The unit of the horizontal axis is yr.

with an amplitude of about 80° and a libration period of about 2×10^4 yr.

(ii) The argument of perihelion of Pluto $\omega_P = \theta_2 = \varpi_P - \Omega_P$ librates around 90° with a period of about 3.8×10^6 yr. The dominant periodic variations of the eccentricity and inclination of Pluto are synchronized with the libration of its argument of perihelion. This is anticipated in the secular perturbation theory constructed by Kozai (1962).

(iii) The longitude of the node of Pluto referred to the longitude of the node of Neptune, $\theta_3 = \Omega_P - \Omega_N$, circulates and the period of this circulation is equal to the period of θ_2 libration. When θ_3 becomes zero, i.e. the longitudes of ascending nodes of Neptune and Pluto

© Royal Astronomical Society • Provided by the NASA Astrophysics Data System

2002MNRAS.336..483I

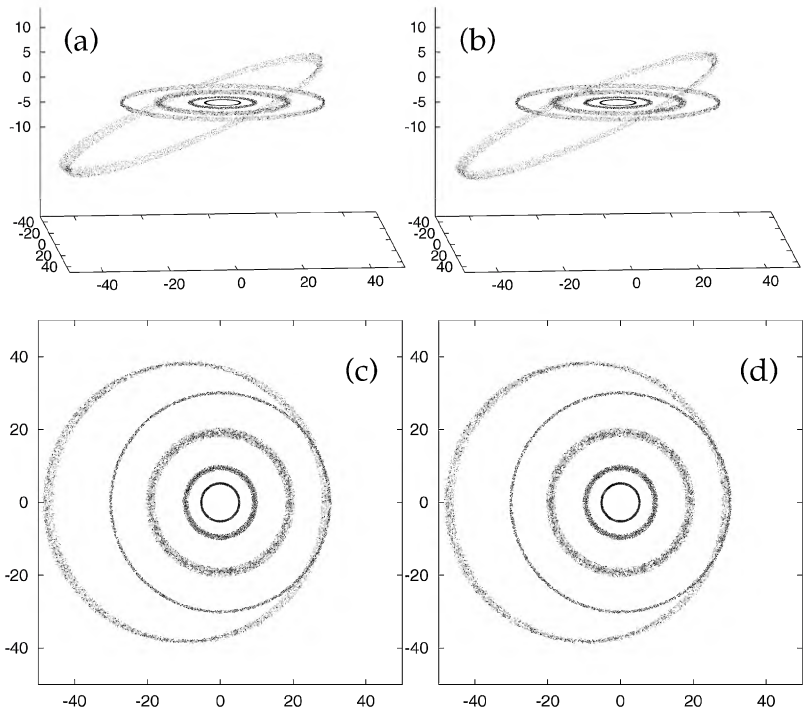

Figure 12. Oblique and vertical views of the outer five planetary orbits in the final parts of the integration $F_{\pm}$. The unit of the axes is au. The xy-plane is set to the invariant plane of the Solar system total angular momentum. (a), (b) The final part of F_{-} ($t = -4.819 \times 10^{10}$ to -5.000×10^{10} yr). (c), (d) The final part of F_{+} ($t = 4.819 \times 10^{10}$ to 5.000×10^{10} yr). In each panel, a total of 23 810 points are plotted with an interval of about 87 611 yr over 1.814×10^{9} yr. In (a) and (c), a rotation is applied to the coordinate system so that the ascending node of Pluto always lies on an x-axis. In (b) and (d), a rotation is applied to the coordinate system so that the perihelion of Pluto always lies on an x-axis. Such transformations make the figures easier to look at since the inclination and eccentricity of Pluto are much larger than those of other planets.

overlap, the inclination of Pluto becomes maximum, the eccentricity becomes minimum and the argument of perihelion becomes 90°. When θ_3 becomes 180°, the inclination of Pluto becomes minimum, the eccentricity becomes maximum and the argument of perihelion becomes 90° again. Williams & Benson (1971) anticipated this type of resonance, later confirmed by Milani, Nobili & Carpino (1989).

(iv) An argument $\theta_4 = \varpi_P - \varpi_N + 3(\Omega_P - \Omega_N)$ librates around 180° with a long period, $\sim 5.7 \times 10^8$ yr.

In our numerical integrations, the resonances (i)–(iii) are well maintained, and variation of the critical arguments $\theta_1, \theta_2, \theta_3$ remain similar during the whole integration period (Figs 14–16). However, the fourth resonance (iv) appears to be different: the critical argument θ_4 alternates libration and circulation over a 10^{10}-yr time-scale (Fig. 17). This is an interesting fact that Kinoshita & Nakai's (1995, 1996) shorter integrations were not able to disclose.

In spite of the fact that the fourth resonance may not remain steady over this long time-span, the Neptune–Pluto system remains completely stable. Thus we find that the fourth resonance may have little effect on the stability of the Neptune–Pluto system.

6 DISCUSSION

What kind of dynamical mechanism maintains this long-term stability of the planetary system? We can immediately think of two major features that may be responsible for the long-term stability. First, there seem to be no significant lower-order resonances (mean motion and secular) between any pair among the nine planets. Jupiter and Saturn are close to a 5:2 mean motion resonance (the famous 'great inequality'), but not just in the resonance zone. Higher-order resonances may cause the chaotic nature of the planetary dynamical motion, but they are not so strong as to destroy the stable planetary motion within the lifetime of the real Solar system. The second feature, which we think is more important for the long-term stability of our planetary system, is the difference in dynamical distance between terrestrial and jovian planetary subsystems (Ito & Tanikawa 1999, 2001). When we measure planetary separations by the mutual Hill radii (R_H), separations among terrestrial planets are greater than $26R_H$, whereas those among jovian planets are less than $14R_H$. This difference is directly related to the difference between dynamical features of terrestrial and jovian planets. Terrestrial planets have smaller masses, shorter orbital periods and wider dynamical separation. They are strongly perturbed by jovian planets that have larger masses, longer orbital periods and narrower dynamical separation. Jovian planets are not perturbed by any other massive bodies.

The present terrestrial planetary system is still being disturbed by the massive jovian planets. However, the wide separation and mutual interaction among the terrestrial planets renders the disturbance ineffective; the degree of disturbance by jovian planets is $O(e_J)$ (order of magnitude of the eccentricity of Jupiter), since the disturbance caused by jovian planets is a forced oscillation having an amplitude of $O(e_J)$. Heightening of eccentricity, for example $O(e_J) \sim 0.05$, is far from sufficient to provoke instability in the terrestrial planets having such a wide separation as $26R_H$. Thus we assume that the present wide dynamical separation among

© Royal Astronomical Society • Provided by the NASA Astrophysics Data System

2002MNRAS.336..483I

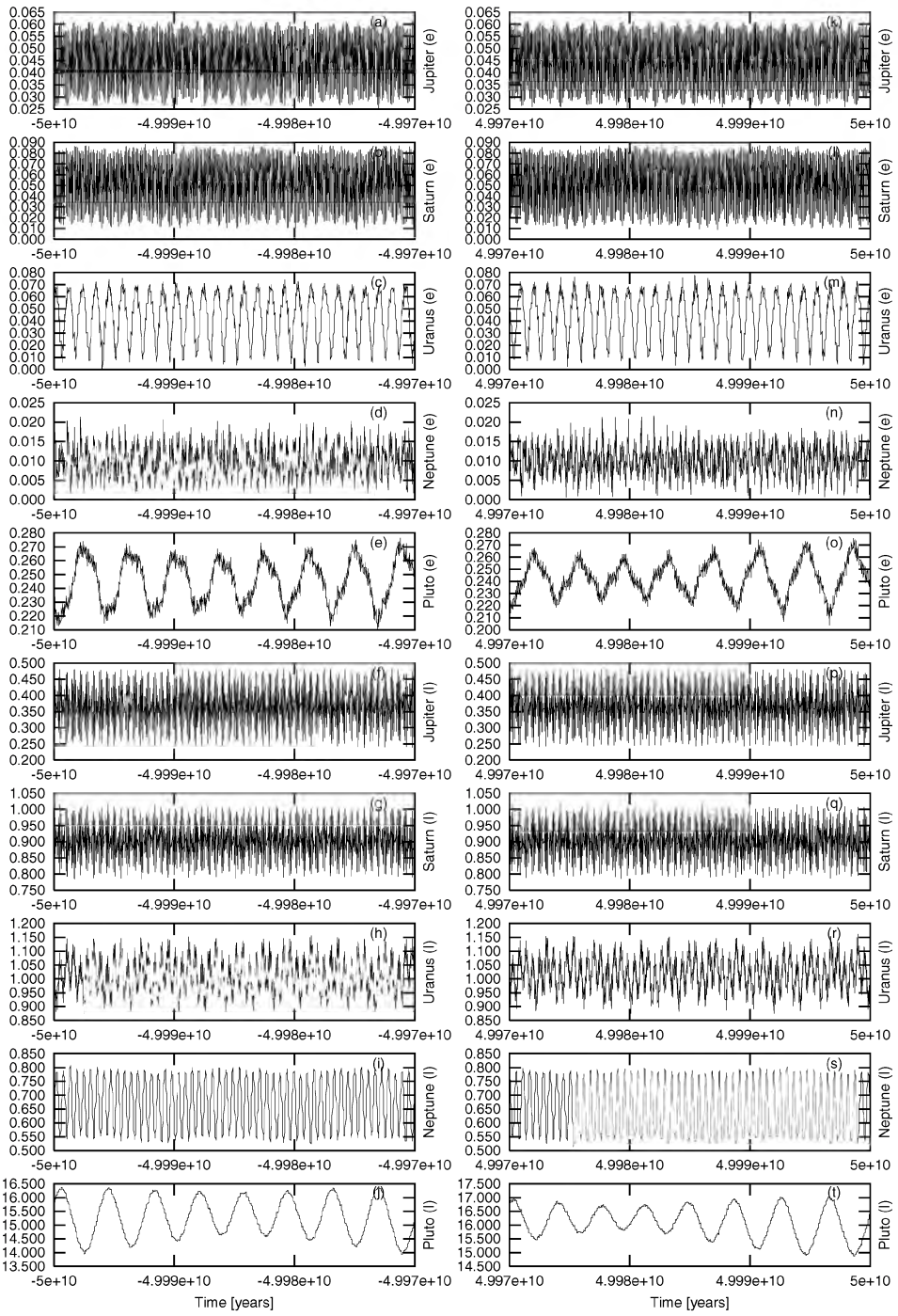

Figure 13. Eccentricities and inclinations of the five outer planetary orbits in the final parts of the integrations $F_{\pm}$. (a)–(e) The eccentricities of Jupiter, Saturn, Uranus, Neptune and Pluto in the final part of the F_{-} integration. (f)–(j) The inclinations of Jupiter, Saturn, Uranus, Neptune and Pluto in the final part of the F_{-} integration. (k)–(o) The eccentricities of Jupiter, Saturn, Uranus, Neptune and Pluto in the final part of the F_{+} integration. (p)–(t) The inclinations of Jupiter, Saturn, Uranus, Neptune and Pluto in the final part of the F_{+} integration. All the elements are reckoned on the Solar system invariable plane with a heliocentric origin.

terrestrial planets ($>26R_{\rm H}$) is probably one of the most significant conditions for maintaining the stability of the planetary system over a 10^9-yr time-span. Our detailed analysis of the relationship between dynamical distance between planets and the instability time-scale of Solar system planetary motion is now on-going.

Although our numerical integrations span the lifetime of the Solar system, the number of integrations is far from sufficient to fill the initial phase space. It is necessary to perform more and more numerical integrations to confirm and examine in detail the long-term stability of our planetary dynamics.

© Royal Astronomical Society • Provided by the NASA Astrophysics Data System

2002MNRAS.336..483I

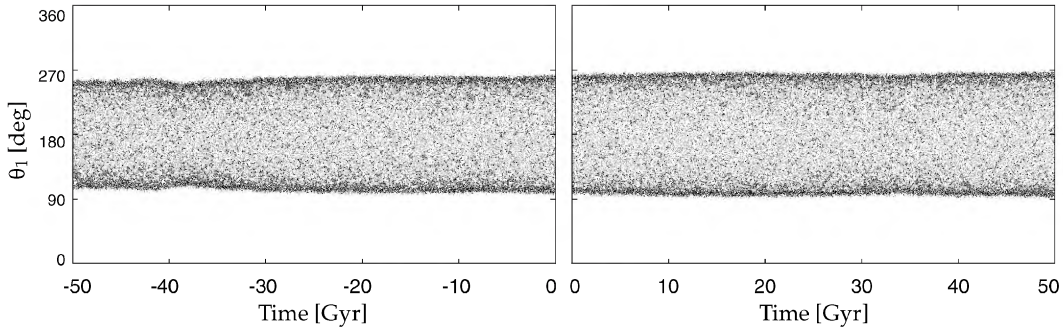

Figure 14. Critical argument θ_1 for F_- (left) and F_+ (right).

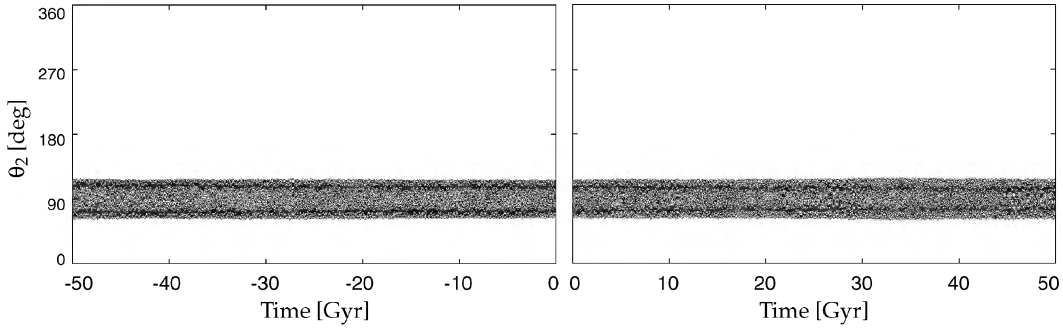

Figure 15. Critical argument θ_2 for F_- (left) and F_+ (right).

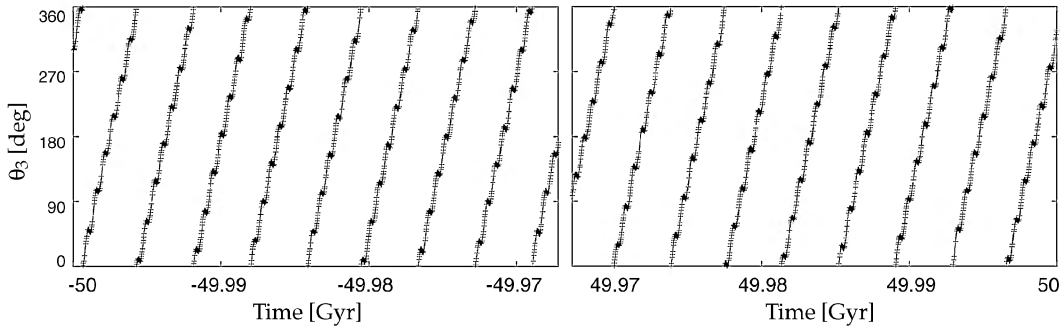

Figure 16. Critical argument θ_3 for F_- (left) and F_+ (right), both in the final part of each integration.

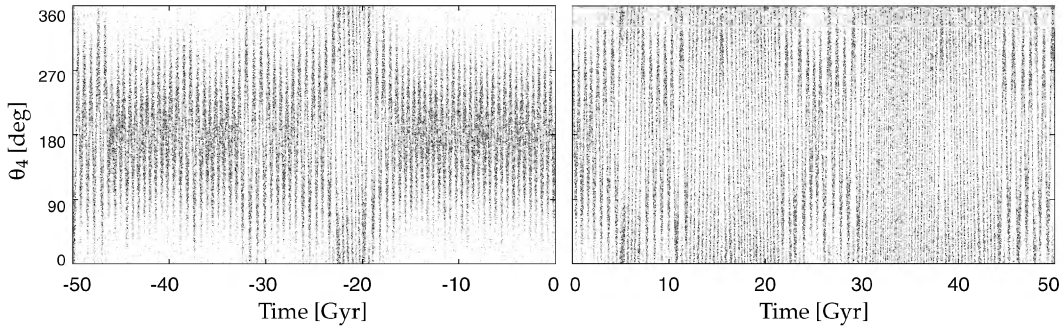

Figure 17. Critical argument θ_4 for F_- (left) and F_+ (right).

© Royal Astronomical Society • Provided by the NASA Astrophysics Data System

2002MNRAS.336..483I

ACKNOWLEDGMENTS

The authors have benefited greatly from stimulating discussions with and encouragement from Hiroshi Kinoshita and Shigeru Ida. A detailed and constructive review by Yolande McLean has considerably improved the English presentation of this paper. The referee also suggested directions that bettered the quality of this paper. This study was supported by the ADAC scientific simulation project, National Astronomical Observatory of Japan (xad01/1999–2001), and the Grant-in-Aid of the Ministry of Education, Science, Sports and Culture of Japan (11740260/1999–2000).

REFERENCES

Berger A.L., 1988, Rev. Geophys., 26, 624
Boccaletti D., Pucacco G., 1998, Theory of Orbits, Vol. 2. Springer-Verlag, Berlin
Brouwer D., Clemence G.M., 1961, Methods of Celestial Mechanics. Academic, New York
Chambers J.E., Wetherill G.W., Boss A.P., 1996, Icarus, 119, 261
Danby J.M.A., 1992, Fundamentals of Celestial Mechanics, 2nd edn. Willmann-Bell, Richmond, VA
Duncan M.J., Lissauer J.J., 1998, Icarus, 134, 303
Fukushima T., 1997a, AJ, 113, 1909
Fukushima T., 1997b, AJ, 113, 2325
Gladman B., 1993, Icarus, 106, 247
Ito T., Tanikawa K., 1999, Icarus, 139, 336
Ito T., Tanikawa K., 2001, PASJ, 53, 143
Kinoshita H., Nakai H., 1996, Earth, Moon Planets, 72, 165
Kinoshita H., Yoshida H., Nakai H., 1991, Celes. Mech. Dyn. Astron., 50, 59
Kozai Y., 1962, AJ, 67, 591
Laskar J., 1988, A&A, 198, 341
Laskar J., 1990, Icarus, 88, 266
Laskar J., 1993, Celes. Mech. Dyn. Astron., 56, 191
Laskar J., 1994, A&A, 287, L9
Laskar J., 1996, Celes. Mech. Dyn. Astron., 64, 115
Laskar J., 1997, A&A, 317, L75
Laskar J., 2000, Phys. Rev. Lett., 84, 3240
Lecar M., Franklin F.A., Holman M., 2001, Annu. Rev. A&A, 39, 581
Milani A., Nobili A.M., Carpino M., 1989, Icarus, 82, 200
Murray N., Holman M., 1999, Sci, 283, 1877
Oppenheim A.V., Schafer R.W., Buck J.R., 1999, Discrete Time Signal Processing. Prentice-Hall, New Jersey
Quinn T.R., Tremaine S., Duncan M., 1991, AJ, 101, 2287
Saha P., Tremaine S., 1992, AJ, 104, 1633
Saha P., Tremaine S., 1994, AJ, 108, 1962
Standish E.M., 1990, A&A, 233, 252
Sussman G.J., Wisdom J., 1988, Sci, 241, 433
Sussman G.J., Wisdom J., 1992, Sci, 257, 56
Williams J.G., Benson G.S., 1971, AJ, 76, 167
Wisdom J., Holman M., 1991, AJ, 102, 1528
Yoshinaga K., Kokubo E., Makino J., 1999, Icarus, 139, 328

This paper has been typeset from a TEX/LATEX file prepared by the author.

© Royal Astronomical Society • Provided by the NASA Astrophysics Data System